

Making the most of available site information for empirical ground-motion prediction

John Douglas, Pierre Gehl

ARN/RIS, BRGM, 3 avenue C. Guillemin, BP 36009, 45060 Orléans Cedex 2, France.

Luis Fabian Bonilla, Oona Scotti

IRSN/DEI/SARG/BERSSIN, BP 17, 92262 Fontenay-aux-Roses Cedex, France.

Julie Régnier, Anne-Marie Duval & Etienne Bertrand

CETE Méditerranée, 56 bd Stalingrad, 06359 Nice Cedex 4, France.

August 28, 2008

Abstract

This article proposes a new framework for the inclusion of site effects in empirical ground-motion prediction equations (GMPEs) by characterizing stations through their one-quarter wavelength velocities and assessed confidence limits. The approach is demonstrated for 14 stations of the French accelerometric network (Réseau Accélérométrique Permanent, RAP). This method can make use of all the available information about a given site, e.g. the surface geology, the soil profile, SPT measurements, near-surface velocity estimated from the topographic slope (Wald and Allen, 2007), depth to bedrock and crustal structure. These data help to constrain the velocity profile down to a few kilometers. Based on a statistical study of 858 real profiles from three different regions (Japan, western North America and France) for generating physically-realistic profiles are generated that comply to the information available for each site.

In order to evaluate the confidence limits for the shear-wave velocity profiles and derived site amplifications for each station, a stochastic method is adopted: several thousands profiles are randomly generated based on parameters derived in the statistical study and the constraints available for each station. Then, the one-quarter wavelength assumption is used to estimate the amplification for each station. It is found that a good knowledge of near-surface attenuation (i.e. κ or Q) is mandatory to obtain precise amplification estimates at high frequencies. Nevertheless, the proposed scheme highlights the important differences in the uncertainties of the site amplifications, depending on the information available for a given station. We suggest that these results could, therefore, be used when developing ground-motion prediction equations (GMPEs) by weighting records from each station depending on the variability in the computed one-quarter wavelength velocities.

This approach relies on the assumption that local site effects are only one-dimensional, which is far from true, especially in sedimentary basins. However, most GMPEs only model one-dimensional site effects, so this is not an issue specific to this study. Finally, a way to improve this technique is to use earthquakes or noise recorded at the very stations to further constrain the shear-wave velocity profiles and to consequently derive more accurate one-quarter wavelength velocities.

1 Introduction

Local site effects have long been recognized as an important factor contributing to variations in strong ground motions (e.g. Boore, 2004). Therefore, the vast majority of empirical ground-motion prediction equations (GMPEs) try to model the differences between ground motions at sites with different local site conditions (e.g. Douglas, 2003). Various different approaches have been followed from simple binary soil/rock classifications (e.g. Berge-Thierry et al, 2003) to the explicit use of shear-wave velocity (e.g. Joyner and Fumal, 1984), and also others such as individual site coefficients for each strong-motion station considered (e.g. Kamiyama and Yanagisawa, 1986). These various procedures are discussed by Douglas (2003). The method that can be chosen is dependent on the quality of readily-available information on site characteristics at strong-motion stations. The explicit use of average (measured or estimated) shear-wave velocity down to 30 m ($V_{s,30}$), with the additional consideration of the effect of basin depth, was adopted by all participants of the PEER Next Generation Attenuation (NGA) project (Abrahamson and Silva, 2008; Boore and Atkinson, 2008; Campbell and Bozorgnia, 2008; Chiou and Youngs, 2008; Idriss, 2008) although Boore and Atkinson (2008) do not find that the basin effect is significant for their model and Idriss (2008) does not include a basin effect in his model. Measuring near-surface wave velocities using conventional methods, such as cross-hole or down-hole techniques, is expensive and time-consuming. Therefore, although such velocities are required, it is unlikely that such measurements will be made at many locations in the near future. In Japan and the United States such measurements are routinely performed. In Europe, however, it is thought that less than 100 strong-motion stations, from a total of over 2953 (European-Mediterranean Seismological Centre, 2007), have had their near-surface wave velocities measured and published.

What all previous approaches have in common is that local site conditions at all stations used to derive GMPEs are assumed to be known to the same detail and with the same accuracy. This is not often true in practice. For example, in the NGA Flat File $V_{s,30}$ is available for some stations based on measurements (from, e.g., cross-hole or down-hole surveys) (for 35% of the records) but for other stations (particularly those outside California) the $V_{s,30}$ values have been

estimated based on local geology and its correlation with $V_{s,30}$. In the NGA Flat File these estimated values are clearly indicated and their estimated standard deviations are higher than those from measurements; however, this difference in the accuracy of $V_{s,30}$ s was not considered by the five GMPE-developer teams.

In addition, the method used to model site effects is invariably limited by the quality of information available for the most poorly characterized station used to derive the GMPEs. For example, Spudich et al (1999) attempted to classify the stations used in their analysis into four categories: hard rock, soft rock, shallow soil and deep soil, but were forced to adopt a simple binary soil/rock classification because information was not available to classify *all* sites into these four categories (29 records, from a total of 142, were from sites classified as ‘unknown soil’ or ‘unknown rock’). In the extreme situation, if, for example, shear-wave velocity profiles were available for all but one site and for that single site the only information available is that it is a ‘rock’ site, a simple binary scheme would have to be used thereby throwing away all the invaluable information available in the velocity profiles (in practice it would be more likely that the data from this single station would be dispensed with for the analysis unless the station provide particularly useful data, e.g. records from very close to the source).

An alternative approach is firstly to use a simple classification technique that is obliged by the lack of information for some stations and then, in a second step, to examine the residuals with respect to more complex site characterization parameters, such as $V_{s,30}$ or basin depth, for those stations with more complete information. This approach has been followed by, for example, Ambraseys (1995) to examine the effect of $V_{s,30}$ and Field (2000) for examining the effect of sedimentary basins on ground motions. When applying such an approach care needs to be taken to account for possible bias in the distributions with respect to other independent variables for stations where detailed site information is available. For example, Boore and Atkinson (2007) show the strong negative correlation between shear-wave velocity and basin depth for data in the NGA Flat File.

None of these techniques to overcome the heterogeneous nature of local site information is completely satisfactory. Therefore, the aim of this article is to propose a new framework that makes use of all the available information about local site conditions to allow the estimation of mean shear-wave velocity profiles and their confidence limits for each station. These profiles can then be used to apply the one-quarter wavelength velocity, $V_{s,\frac{1}{4}}$, method to model site effects within GMPEs (Joyner and Fumal, 1984) and through a weighting scheme within the regression procedure the different confidence limits of the $V_{s,\frac{1}{4}}$ s can be accounted for. The following two sections describe the proposed procedure including the method to generate a distribution of possible shear-wave velocity profiles for each station. Then in Section 4 the

technique is applied. The technique is then applied to 14 stations of the French accelerometric network (Réseau Accélérométrique Permanent, RAP). Following this, a weighting scheme for use in regression analysis when deriving GMPEs using this approach is proposed. The article closes with a discussion of the merits and disadvantages of the proposed method to evaluate the shear-wave velocity profiles, the $V_{s, \frac{1}{4}}$ s and site amplifications using the one-quarter wavelength assumption.

2 Proposed method

In the proposed procedure local site conditions are characterized using the average near-surface wave velocities down to a depth equal to one-quarter the wavelength of the wave of interest (e.g. Joyner et al, 1981). Joyner et al (1981), Boore and Joyner (1991) and Boore and Joyner (1997) show that the quarter-wavelength method for assessing site amplification yields good estimates of the site amplification without the requirement of complex computation. The equation to estimate the amplification, $A(f)$, (where f is frequency) at a site is (e.g. Boore, 2003):

$$\begin{aligned}
 A(f) &= \sqrt{\frac{\rho_s \beta_s}{\bar{\rho}(f) \bar{\beta}(f)}} & (1) \\
 \text{where } \bar{\rho}(f) &= \frac{1}{z(f)} \int_0^{z(f)} \rho(z) dz \\
 \bar{\beta}(f) &= z(f) \left[\int_0^{z(f)} \left(\frac{1}{\beta(z)} \right) dz \right]^{-1} \\
 z(f) &= \frac{\bar{\beta}(f)}{4f}
 \end{aligned}$$

where $\beta(z)$ is the shear-wave velocity at depth z , $\rho(z)$ is the density at depth z and β_s and ρ_s are the shear-wave velocity and the density at the source, respectively. For this study, the `site_amp` program (Boore, 2005) is used to compute site amplification using this method.

This technique models the effect of the impedance contrast between the underlying bedrock (with a high material velocity) and the softer surface deposits (with a lower material velocity). As waves travel vertically from one medium to another the amplitudes of the waves must increase, if the velocity is decreasing towards the surface and losses due to reflection, scattering and anelastic attenuation are neglected, since the energy along a tube of rays is constant. Using the quarter-wavelength approximation predicts the period of the first peak of the amplification curve if it is assumed that the velocity is for a uniform layer of thickness equal to the depth to which the average was estimated.

By using the one-quarter wavelength approach we make the assumption of one-dimensional linear site response, which is a common assumption in the derivation of empirical GMPEs.

However, this assumption means that predicted site amplifications derived using this approach are unlikely to be accurate for sites with strong two- or three-dimensional site effects (e.g. those stations in sedimentary basins) or for sites where nonlinear soil response is possible for large amplitude ground motions. Since nonlinear soil response only becomes apparent for peak ground accelerations (PGA) greater than 0.1–0.2g (e.g. Beresnev and Wen, 1996) site amplification for the majority of records should be accurately predicted despite neglecting nonlinearity.

For this article the one-quarter wavelength technique to assess site amplifications is preferred to full one-dimensional site response analysis using, for example, the Haskell-Thompson method because the associated one-quarter wavelength velocities, $V_{s,\frac{1}{4}}$ s, can be readily incorporated into the functional form of the GMPEs (Joyner and Fumal, 1984). Site amplifications derived from full 1D site response analysis could be directly incorporated into GMPEs but such GMPEs would be difficult to use in practice for sites without assessed amplifications. As will be shown in Section 4 $V_{s,\frac{1}{4}}$ can be estimated using our approach even for sites where the knowledge of the sub-soil structure is limited (e.g. those sites only defined by site category). As will be shown in Section 6 (and previously shown in Boore and Joyner (1991)) the one-quarter wavelength simplification for estimating site amplification does not allow the prediction of the resonant peaks due to multiple reflections of waves, which can be predicted by full 1D site response analysis.

To apply this method shear-wave velocity estimates down to a few km (to compute site amplifications up to long periods, e.g. 10s) for every site considered need to be available. Except for a few special sites, such as Cajon Pass (USA) (e.g. Abercrombie, 1997), measured shear-wave velocities are not available beyond a few tens or hundreds of meters, if at all. However, other information is available that can be used to approximate the shear-wave and density velocity profiles down to the one-quarter wavelength depth. The types of information available to estimate the profiles are discussed in the following paragraph. This information will allow a distribution of possible velocity and density profiles to be defined from which the distribution of possible $V_{s,\frac{1}{4}}$ s can be estimated. When more constraints are available, for example when a measured shear-wave velocity profile exists, the distribution of $V_{s,\frac{1}{4}}$ for that station will be narrower than when few constraints are available, for example when the profile is based only on local geological information. Strong-motion data from stations with well-defined $V_{s,\frac{1}{4}}$ s should be given more weight in the regression analysis than those data from stations with few constraints on these velocities.

Table 1 lists the information that is sometimes available to help constrain shear-wave velocity and density profiles down to a few kms. Obviously not all these sources of information

are available for every site. For example, information relying on on-site measurements (e.g. SPT results) are rarely available for strong-motion stations. However, some of these data (e.g. topographic slope) can be calculated based on remote-sensing information and therefore they exist for all sites.

[Table 1 about here.]

This proposed method, therefore, has the ability to incorporate all the available information on local site conditions into the derivation of ground motion estimation equations rather than, as is done at present, be forced to default to a crude site classification scheme because of a lack of information for some stations. It accounts for the fact that the quality of local site information varies significantly between stations — a heterogeneity that is not normally considered when deriving GMPEs. This method will not significantly improve site-specific earthquake-specific site response estimates because, as Boore (2004) shows, these estimates require detailed knowledge of the source and the three-dimensional structure beneath the station. However, it should improve overall estimates of average site response and consequently empirical ground-motion estimates.

3 Generation of shear-wave and density profiles

In this study, a large set of physically-realistic profiles is generated that can then be reduced by the application of constraints from information available at each strong-motion station considered. The generation of these profiles has been made using a Monte Carlo technique with input parameters coming from the analysis of many (858) measured profiles, which are assumed to be a representative sample of possible near-surface velocity profiles. The random generation of velocity profiles has been performed in a few previous studies (e.g. Bernreuter et al, 1986; Anderson et al, 1996) using different approaches than adopted here. Three sets of profiles are used in this study: those collected and disseminated by David Boore for sites in western North America (http://quake.wr.usgs.gov/~boore/data_online.htm, 277 sites), those collected by Julien Rey for sites in France (43 sites) and those compiled by Guillaume Pousse for Kik-Net strong-motion stations in Japan (538 sites).

These profiles were normalized by dividing the velocity in each layer by the velocity in the surface layer. Then, the normalized velocity slope between two layers was calculated, using the following equation:

$$\text{slope}(n) = \frac{V_{n+1} - V_n}{H_n} \quad (2)$$

where V_n is the normalized velocity at layer n and H_n the thickness of layer n . The 858 profiles lead to 3026 normalized slopes (one for each layer). Then, we extracted the depth and the maximum velocity for each profile, as well as the maximum and minimum thickness of each layer and the surface velocity. The gross characteristics of the profiles collected are summarized in Figures 1 and 2. These figures show that the vast majority of profiles are of soft soil sites with surface shear-wave velocities less than 400 m/s and that information is generally only available for the first 100 m or less with a resolution generally higher than 50 m. Figure 3 shows the computed normalized slopes against depth.

To check that the parameters extracted from the observed profiles were not correlated, we performed a principal component analysis on characteristics such as slope, layer depth, layer thickness or velocity (Table 2). This analysis shows that the slope is poorly correlated with the other variables and, thus, here we neglect the correlation between the slope and other parameters.

[Figure 1 about here.]

[Figure 2 about here.]

[Figure 3 about here.]

[Table 2 about here.]

The gross characteristics of the profiles are approximatively distributed according to these distributions:

- maximum depth D : log-normal distribution ($\phi(x) = \frac{1}{x\beta\sqrt{2\pi}} \exp[-\frac{(\ln(x)-\alpha)^2}{2\beta^2}]$, where x is a random variable and $\phi(x)$ is the probability density function) with parameters mean $\alpha = 4.08$ and standard deviation $\beta = 0.70$;
- minimum thickness H_{min} : normal distribution ($\phi(x) = \frac{1}{\sigma\sqrt{2\pi}} \exp[-\frac{(x-\mu)^2}{2\sigma^2}]$) with mean $\mu = 4.3$ m and standard deviation $\sigma = 6.6$ m;
- maximum thickness H_{max} : normal distribution with $\mu = 37.6$ m and $\sigma = 39.5$ m;
- surface velocity V_0 : log-normal distribution with $\alpha = 5.28$ and $\beta = 0.49$.

The maximum velocity V_{max} depends strongly on the depth D of the profile, therefore it was decided to divide the profiles into three groups:

- $D \leq 50$ m: normal distribution of V_{max} with $\mu = 1091.8$ m/s and $\sigma = 519.3$ m/s

- $50 < D \leq 100$ m: normal distribution of V_{max} with $\mu = 1141.8$ m/s and $\sigma = 602.0$ m/s
- $D > 100$ m: normal distribution of V_{max} with $\mu = 1240.7$ m/s and $\sigma = 648.5$ m/s

Thanks to all these distributions, it was possible to generate stochastic profiles, using the following method:

- random selection of a depth D , based on its statistical distribution;
- from the surface to the depth D , generation, assuming a uniform distribution, of layers whose thicknesses are constrained by H_{min} and H_{max} , both parameters being chosen from their statistical distributions;
- random selection of a surface velocity V_0 , based on its statistical distribution;
- for each layer, generation of slope values, based on the empirical distribution (the slope values were found not to closely fit any tested statistical distribution so their empirical distribution was used);
- with the slope and the surface velocity V_0 , generation of the velocity of each layer down to depth D .

In order to avoid unrealistic results, the profiles were constrained using the following criteria:

- the velocity of a layer cannot be less than 50 m/s; and
- the velocity cannot exceed the maximum velocity V_{max} , which is randomly selected from the statistical distribution.

Thus, this method can generate velocity profiles down to depth D (usually between 50 and 200 m). However, this approach cannot be used for deeper layers because it is based on shallow profiles and using these values for greater depths leads to unrealistic profiles. It was therefore decided to define much looser constraints on the velocity profile between the depth D and 10 km. First of all, in order to reflect the homogeneity of the medium at these depths, much thicker layers were selected, between 50 and 500 m. The velocity contrast between two layers can be defined by:

$$R_n = \frac{V_{n+1}}{V_n} \quad (3)$$

The values of the impedance factor R_n are based on the 858 profiles, leading to a log-normal distribution with parameters $\alpha = 0.41$ and $\beta = 0.48$. We acknowledge that the methodology used for the deeper layers is based on information extrapolated from the shallow parts of the

profile. This assumption is a reasonable way to construct a profile between the upper layers, where statistical results from boreholes can be used, and the lower layers where velocities from crustal structural models are available. Finally, in order to avoid unrealistic results, it was decided to keep only the profiles where:

- the velocity does not exceed 3800 m/s; and
- the velocity is not less than the value at the depth D .

Figure 4 summarizes the procedure that was used to generate the profiles. By visual inspection of numerous simulations, the profiles generated using this approach were seen to show similar characteristics to those in the set of 858 observed profiles. Even though some individual profiles generated by this approach may be unrealistic, the average characteristics of the profiles (which affect amplifications predicted by the one-quarter wavelength method) should match those observed in reality. It is important that there are sufficient constraints in the profile simulation method to exclude physically impossible profiles but on the other hand sufficient freedom must be given so as not to underestimate the width of the confidence limits of the predicted $V_{s, \frac{1}{4}}$.

[Figure 4 about here.]

3.1 Constraints on the profiles

The method above can be used to generate any kind of velocity profile, for any kind of site. Yet, the main goal of this study is to investigate the effects of more accurate velocity profiles (i.e. stations with more information) on the variability of the amplification curve and $V_{s, \frac{1}{4}}$, which will be used within the GMPEs.

We have selected the five following types of information that can be useful to constrain the profiles.

- Surface velocity, V_0 : this constraint is added in the method above by selecting the same V_0 for all the simulated profiles.
- Mean velocity down to 30 m, $V_{s,30}$: this data can be obtained with the site class (e.g. Eurocode 8 classification (Comité Européen de Normalisation (CEN), 2005)) or approximated using the topographic slope (Wald and Allen, 2007). If the approximate range of $V_{s,30}$ is known, it is easy then to reject the profiles that do not fall into the desired range.
- The velocity profile down to a certain depth: this can be obtained from geological logs and geotechnical techniques using correlations between SPT and/or soil/rock type and V_s .

To use this constraint, we apply the same procedure as for V_0 , except down to a certain depth. Then the profile is again generated using random parameters. For sites with soil profiles the empirical relations between soil type and shear-wave velocity developed by Ohta and Goto (1978) (their equations VII and VIII) have been used in combination with Table 5.1 of Dowrick (2003) to convert soil/rock descriptions to shear-wave velocities.

- The depth to the bedrock: with this information, we can assume that, below a given depth, the velocity will not be less than a certain value. This constraint may also be added to the model, if available.
- The mean crustal velocities: with these data, it is possible to constrain the velocity at depths of greater than 1 km.

A coefficient of variation of 10% is applied to V_s estimates if they come from geological logs or geotechnical techniques and a coefficient of variation of 25% is assumed if the V_s estimates are deduced from empirical relations between soil type and shear-wave velocity (Ohta and Goto, 1978).

3.2 Generation of density profiles

The density does not play a predominant role in the variability of amplification curves. Thus, we used the velocity values to estimate the density using this linear relation (Boore and Joyner, 1997):

$$\rho(V_s) = 2500 + \frac{V_s - 300}{3500 - 300} \cdot (2800 - 2500) \quad (4)$$

Boore and Joyner (1997) state that this relationship is valid for V_s between 300 m/s and 3.5 km/s. Some of our profiles include V_s outside this range (down to about 100 m/s and up to 3.8 m/s) but this should not have a significant impact on the results. For example, for $V_s = 100$ m/s Equation 4 gives $\rho = 2481$ kg/m³, which is very similar to the recommendation of Boore and Joyner (1997) of 2500 kg/m³ for $V_s < 300$ m/s.

3.3 Generation of amplification curves

After the simulation of thousands of possible velocity and density profiles, the profiles that do not conform to the constraints applicable for a station are excluded thereby leaving a set of possible profiles for that site. This subset of profiles is then used within the one-quarter wavelength approach to estimate the possible site amplifications at that site. The reduction in the uncertainty in the estimated site amplification after applying constraints can

then be quantified by comparing these amplifications with those computed using the entire set of generated profiles.

The one-quarter wavelength method also requires the shear-wave velocity V_s and the density ρ in the source region. We chose to take $V_s = V(10 \text{ km})$ for each profile thereby assuming a hypocentral depth of 10 km. As shown above, the density in the source region can be deduced from the velocity.

Near-surface attenuation can be approximated using (Anderson and Hough, 1984): $\exp -\pi\kappa f$, where κ is a spectral decay parameter that is commonly assumed to be a constant for a given station although a weak positive dependence on distance has sometimes been observed (e.g. Anderson and Hough, 1984). The amplification $A(f)$ is then multiplied by the near-surface attenuation, approximated using κ , to obtain an overall amplification. As is standard practice (e.g. Boore and Joyner, 1997) this attenuation filter is applied to the entire frequency range even though κ is estimated based on the high-frequency part of Fourier amplitude spectra and, in addition, κ is assumed to be independent of frequency. In this study, we use a mean value of κ for each profile, based on the empirical relationship connecting $V_{s,30}$ and κ presented by Silva et al (1998): $\log \kappa = 1.6549 - 1.0930 \log V_{s,30}$. In order to model uncertainties in the κ s estimated by this equation we have computed a standard deviation of 0.25 from the data points presented in Figure 21 of Silva et al (1998), which has been used to generate a κ for each profile. To keep the κ s used within a physically-realistic range (e.g. Silva et al, 1998, Figure 21) values less than 0.005 or greater than 0.15 were rejected. The large variability in κ estimated from the $V_{s,30}$ is because near-surface attenuation modeled by κ is affected by more than the top 30 m at a site. In the absence of a better method to estimate κ from a given shear-wave velocity profile the large range of κ s given by this approach have been accepted even though it could lead to overestimating the uncertainty in the site response for frequencies greater than about 1 Hz, where the effect of attenuation modeled by κ becomes important. An alternative would be to use a attenuation (Q) profile, possibly estimated based on empirical relationships between V_s and Q (e.g. Barker and Stevens, 1983); however, there are few such correlations and they are also associated with large uncertainties.

4 Application of proposed approach to RAP stations

Fumal and Tinsley (1985) present a method and relations for the estimation of one-quarter wavelength velocity for sites in California; a similar technique is applied here for the French sites selected. Recently a RAP working group compiled information on local site conditions at most of the RAP stations (Groupe de Travail RAP, 2007), which are selected here for an appli-

cation of the method proposed above. The type, quality and quantity of information for these stations could be considered representative of the situation for most strong-motion networks, particularly those outside California or Japan, where routine borehole velocity measurements have not been conducted. From the investigated sites we have selected 14 stations that have a range of data available and are from various regions of metropolitan France, see Table 3.

[Table 3 about here.]

Based on the information available for each of the 14 RAP stations (Table 3) stochastic shear-wave velocity profiles were generated using the approach described above. The mean and the 10 and 90th percentile profiles for the 14 stations are displayed in Figure 5. The profiles for stations such as NALS with available detailed soil profiles that can be converted into approximate shear-wave velocities are, as expected, well constrained down to the bottom of the profile. In contrast profiles for stations such as OGMU, with few available constraints on the near-surface shear-wave velocities, show much greater dispersion. There is limited information available to constrain the profiles below the end of the boreholes (at about 50 m) and above the start of the available crustal structural models (at 1 or 2 km) and, hence, profiles for all stations show a wide dispersion within this depth range.

[Figure 5 about here.]

Figure 5 shows that some profiles (e.g. NALS, NLIB, NPOR and NPOR) contain velocity inversions, which is explained by negative slopes (Equation 2) as shown in Figure 3. In addition, Figure 3 shows that negative slopes can even be found in deeper layers (e.g. below 100 m depth), which corresponds to the velocity inversions found in some profiles.

Using the stochastic velocity and density profiles amplification curves for each of the sites were computed using the one-quarter-wavelength technique. Figure 6 shows the mean and 10 and 90th percentile amplification curves for the 14 stations. As is expected the amplifications at stations with measured or, in the case of RAP stations, estimated near-surface velocity profiles are more accurately defined (e.g. NALS) than those at stations without such constraints (e.g. PYFO). Surprisingly, however, even when detailed soil profiles are available (from which shear-wave velocities can be estimated) site amplifications at high frequencies still show large dispersion. For example, the 10 and 90th percentiles for the amplification at 10 Hz at NALS are roughly 0.2 and 1.5 (Figure 6), which is surprising since for this site and 10 Hz the one-quarter wavelength is roughly 5 m and, hence, it would be thought that a shear-wave velocity profile down to 39 m would be adequate to precisely define the amplification.

[Figure 6 about here.]

The reason that the amplifications are not more precisely defined when near-surface velocity profiles are available is that near-surface attenuation (here modeled by κ) is not known for these stations and so it is estimated using the equation of Silva et al (1998) with its associated uncertainty. It is this uncertainty that leads to the dispersion in the predicted amplification curves for high frequencies. Figures 7 and 8 show the effect of neglecting the uncertainty in the estimation of κ from $V_{s,30}$ using the equation and data of Silva et al (1998) for two stations with detailed estimated shear-wave velocity profiles: NALS and OGSR. When κ is assumed to be precisely known (left-hand graphs) the computed amplification curves are almost exactly known for frequencies greater than roughly 1.5 Hz but when uncertainty in κ is included (right-hand graphs) there is considerable uncertainty in the calculated site amplifications. Anderson et al (1996) examine the influence on ground motions of the top 30 m and they believe that near-surface attenuation is more important than details of the velocity profile for controlling high-frequency ground motions. The results of this study show the need to measure the near-surface attenuation at strong-motion stations in addition to near-surface velocities if it is hoped to calculate precise site amplifications through modeling of site response.

[Figure 7 about here.]

[Figure 8 about here.]

Drouet et al (2008) invert ground motions recorded by a selection of RAP stations to retrieve source, path and site parameters for two regions of France: the Pyrenees and the Alps. Within their analysis they included records from seven of the 14 stations studied here. Figure 9 compares the site amplifications and their uncertainties retrieved by Drouet et al (2008) using their inversion technique to those derived using the method followed here. The match between the two sets of amplifications shown in Figure 9 is poor for all of the stations. In general, the method followed here gives higher amplifications than the approach of Drouet et al (2008), except for NROC and OGDH where the amplifications of Drouet et al (2008) are much higher. The amplifications computed by Drouet et al (2008) are relative to an average of sites whose amplification is minimal whereas here the amplifications calculated are absolute with respect to the source. Therefore, the two sets of amplifications are not directly comparable. In addition, the procedure followed here assumes one-dimensional linear site response and therefore it cannot fully model site response at stations affected by two- or three-dimensional effects, such as those in sedimentary valleys (e.g. OGDH and OGSR, which are in the Grenoble sediment basin, and NROC which is on sediments in Nice) whereas the observational method of Drouet et al (2008) may pick up such effects. The width of the confidence limits on the mean site amplification given by the two methods are similar.

[Figure 9 about here.]

Rodriguez-Marek et al (1999) (and others) find that the consideration of the depth to bedrock within site classification leads to a reduction in the standard deviation of site amplification estimates. In this study this common observation has been tested for two stations: NALS on shallow sedimentary layers in Nice and OGSR in a deep sedimentary basin in Grenoble. In addition, the increase in the accuracy of the predicted site amplification through the use of additional constraints (e.g. near-surface shear-wave velocity profile) has been tested. Figure 10 shows four computed site amplification curves (with their confidence limits) for the NALS station when: I) all available data (near-surface profile, depth to bedrock and crustal structure) has been used, II) when the near-surface profile has been replaced by the measured $V_{s,30}$ and V_0 , III) when the depth to bedrock has been removed as a constraint and IV) when only the $V_{s,30}$ and the crustal structure have been retained as constraints. Figure 11 shows the four computed amplification curves (with their confidence limits) for the OGSR station for the same four sets of constraints. These two figures show (by comparing the results for cases I and II), as expected, that a near-surface profile helps to narrow the confidence limits of the site amplification curve for frequencies around 1 Hz but due to the uncertainty in near-surface attenuation the accuracy of high-frequency (> 2 Hz) amplifications is not significantly improved over the case when a measured $V_{s,30}$ is used instead. The inclusion of a depth to bedrock constraint (compare cases II and III) helps reduce the uncertainty in the low frequency (< 1 Hz) amplification curves, confirming the conclusions of previous studies showing the importance of depth to bedrock when computing site response.

[Figure 10 about here.]

[Figure 11 about here.]

It is possible to use our approach to develop generic amplification curves for the site classes defined in earthquake design codes, e.g. Eurocode 8 (EC8) (Comité Européen de Normalisation (CEN), 2005) in which site classes are based on $V_{s,30}$: A, $V_{s,30} > 800$ m/s; B, $360 \leq V_{s,30} \leq 800$ m/s; C, $180 \leq V_{s,30} < 360$ m/s; and D, $V_{s,30} < 180$ m/s. The four generic profiles and amplification curves corresponding to EC8 site classes A, B, C and D generated using our approach and the appropriate constraint on $V_{s,30}$ are presented in Figures 12 and 13, respectively. Cotton et al (2006) present equations for the creation of profiles, based on the generic rock profiles of Boore and Joyner (1997), for a given $V_{s,30}$ to adjust GMPEs derived for different rock conditions. Our results are compared in Figures 12 and 13 to profiles produced by the approach of Cotton et al (2006) and their corresponding amplifications. These comparisons show that the method developed in this article enables the construction of realistic

velocity profiles and are similar to the ones procedure by the approach of Cotton et al (2006) although, also, our approach allows the estimation of the confidence limits of the profiles. In addition, the development of generic profiles for each site class enables our approach to be used to evaluate the GMPEs derived using $V_{s,\frac{1}{4}}$ even for sites with little information available on the sub-soil structure. When using these generic profiles (or associated site amplifications) account should be made of the associated accuracy of the $V_{s,\frac{1}{4}}$ estimates so that confidence limits of the predicted ground motions can be correctly assessed.

[Figure 12 about here.]

[Figure 13 about here.]

5 Regression analysis using $V_{s,\frac{1}{4}}$ s of varying accuracies

The $V_{s,\frac{1}{4}}$ s derived using the procedure given above are associated with different variabilities depending on the data available to constrain the velocity and density profiles. Therefore when using these velocities (or the amplifications) in the derivation of GMPEs weights should be applied to account for their varying accuracies. As discussed by Draper and Smith (1998, pp. 223–229) weighted least squares should be applied when the *observations* have different variances. However, this is not directly comparable to the situation considered here, where the variances (accuracies) of one of the *input* variables are not the same.

Huo and Hu (1991) describe an approach to account for errors in magnitude and distance when developing GMPEs and Rhoades (1997) presents a regression method that accounts for differences in variances of magnitudes between earthquakes used to derive GMPEs. The technique of Rhoades (1997) is not directly applicable here since his formulation is based on assuming the errors in magnitude affect the inter-event terms whereas errors in $V_{s,\frac{1}{4}}$ will affect the intra-event terms. In general, regression analysis using measurement-error models (e.g. Fuller, 1987) allows account to be made of errors in the independent variables, such as $V_{s,\frac{1}{4}}$. This type of approach could be used to deal with differences in the variances of the estimates of $V_{s,\frac{1}{4}}$ (the one-quarter wavelength velocity) for each station. Currently there is insufficient strong-motion data available from the RAP to develop robust GMPEs and therefore, in this article, no regression analysis has been attempted. Nevertheless, Table 4 presents the computed mean $V_{s,\frac{1}{4}}$ s and their 10 and 90th percentile confidence limits for the 14 RAP stations and the four EC8 site classes for different spectral periods. Such information would be the basis of the derivation of GMPEs using $V_{s,\frac{1}{4}}$ (Joyner and Fumal, 1984) and a regression procedure to account for the variation in the accuracies of the velocities.

[Table 4 about here.]

6 Conclusions

In this article we have estimated the shear-wave velocity profiles and computed the $V_{s, \frac{1}{4}}s$ (Joyner and Fumal, 1984) and site amplifications (and their confidence limits) for 14 stations in the RAP strong-motion network of France. In this application most of the available data to constrain the possible shear-wave velocity profiles has been used. To compute a set of realistic shear-wave profiles a stochastic profile simulation technique was developed based on statistical descriptions of the characteristics of 858 measured profiles from western North America, France and Japan. The advantage of this is that when the computed $V_{s, \frac{1}{4}}s$ (or site amplifications) are used to develop GMPEs the common assumption of equal quality and quantity of site information is no longer required. Data from stations should be weighted within the regression analysis based on the accuracy of the computed $V_{s, \frac{1}{4}}s$. Such a weighted regression analysis is planned for a future extension of this study.

This proposed method, therefore, has the ability to incorporate all the available information on local site conditions into the derivation of ground motion estimation equations rather than, as is done at present, be forced to default to a crude site classification scheme because of a lack of information for some stations. It accounts for the fact that the quality of local site information varies significantly between stations — a heterogeneity that is not normally considered when deriving GMPEs. This method will not significantly improve site-specific earthquake-specific site response estimates because, as Boore (2004) shows, these estimates require detailed knowledge of the source and the three-dimensional structure beneath the station. However, it should improve overall estimates of average site response and consequently empirical ground-motion estimates.

From this study a number of important conclusions on the estimation of site amplifications based on modeling using geophysical data can be made. It has been demonstrated that precise amplification estimates at high frequencies rely on accurate estimates of near-surface attenuation (i.e. κ or Q), which is not usually measured, as well as near-surface shear-wave velocity. In addition, the application of depth to bedrock constraints can improve the accuracy of amplification curves for frequencies around 1 Hz.

The presented technique, however, has three main drawbacks. Firstly, by using the one-quarter wavelength approach we assume one-dimensional linear site response, which is a common assumption when deriving empirical GMPEs. However, this assumption means that predicted site amplifications derived using this approach are unlikely to be accurate for sites with

strong two- or three-dimensional site effects (e.g. those stations in sedimentary basins) or for sites where nonlinear soil response is possible for large amplitude ground motions. Since nonlinear soil response only becomes apparent for peak ground accelerations (PGA) greater than 0.1–0.2 g (e.g. Beresnev and Wen, 1996) site amplification for the majority of records should be accurately predicted despite neglecting nonlinearity.

The second disadvantage of the proposed approach is that it does not currently make use of site response information coming from analysis of recorded earthquakes or ambient vibrations, such as horizontal/vertical (H/V) spectral ratios (e.g. Duval et al, 2001; Fukushima et al, 2007). This information could be useful in constraining the shear-wave velocity profiles at depths beyond the end of information coming from boreholes. The disadvantage of not making use of this information has been demonstrated here by the generally poor match between computed site amplifications and those presented by Drouet et al (2008) for seven common stations. However, it should be possible to make use of this information by conducting full one-dimensional site response analysis (rather than making the one-quarter wavelength approximation) for the set of generated profiles and then rejecting those profiles whose site response does not match the observations coming from recorded data. A benefit of the one-quarter wavelength approach, however, is that the one-quarter wavelength velocities ($V_{s,\frac{1}{4}}$) obtained from the profiles can be easily included within the functional form of the derived GMPEs through the addition of a term: $k \log(V_{s,\frac{1}{4}}/V_0)$, where k and V_0 are coefficients to be found by regression analysis, which is based on the physics of site response (Joyner and Fumal, 1984). Using the average velocities down to a depth of one-quarter wavelength neglects the effect of variation in the velocity structure below this depth, which at high frequencies would mean neglecting variations below a few tens of metres.

As an example of the benefit of full one-dimensional site response analysis when making use of results of H/V spectral ratios (or other estimates of the site response) to better constrain profiles Figure 14 compares the amplification curves computed using the Haskell-Thompson approach with those estimated using the one-quarter wavelength approximation for the OGDH station in the Grenoble basin. This comparison shows that the Haskell-Thompson approach predicts this site’s fundamental frequency (at about 0.2 Hz) whereas the one-quarter wavelength approximation does not. Consequently if estimates of a site’s fundamental frequency are available from observational data, such as H/V spectral analysis, the one-quarter wavelength approximation would not make use of this information. The OGDH amplification curve for this station derived using the Haskell-Thompson approach (Figure 14) compares well with the amplifications estimated by Drouet et al (2008) (Figure 9). This example demonstrates the final principal disadvantage of basing our approach on the one-quarter wavelength assumption,

i.e. the site response at stations underlain by large impedance contrasts, with consequently site responses featuring multi-reflections, could be poorly characterized. Nevertheless, we prefer the one-quarter wavelength approach for our procedure due to the ease with which the $V_{s, \frac{1}{4}S}$ can be introduced into empirical GMPEs.

[Figure 14 about here.]

7 Acknowledgments

This study was funded by BRGM research and public service projects and a grant from the Réseau Accélérométrique Permanent (RAP) of France. We thank: the RAP working group on geotechnical site characterization for their data collection tasks and Philippe Guéguen for providing this information; Julien Rey, Guillaume Pousse and David Boore for providing their compilations of shear-wave velocity profiles; Sylvette Bonnefoy-Claudet for advice and for providing a copy of Vallon (1999); and Stéphane Drouet for sending us the numerical values of his amplification curves. Finally, we thank two anonymous reviewers and associate editor, Julian Bommer, for their careful and detailed reviews, which led to significant improvements to this article.

References

- Abercrombie RE (1997) Near-surface attenuation and site effects from comparison of surface and deep borehole recordings. *Bulletin of the Seismological Society of America* 87(3):731–744
- Abrahamson N, Silva W (2008) Summary of the Abrahamson & Silva NGA ground-motion relations. *Earthquake Spectra* 24(1):67–97, DOI 10.1193/1.2924360
- Ambraseys NN (1995) The prediction of earthquake peak ground acceleration in Europe. *Earthquake Engineering and Structural Dynamics* 24(4):467–490
- Anderson JG, Hough SE (1984) A model for the shape of the Fourier amplitude spectrum of acceleration at high frequencies. *Bulletin of the Seismological Society of America* 74(5):1969–1993
- Anderson JG, Lee Y, Zeng Y, Day S (1996) Control of strong motion by the upper 30 meters. *Bulletin of the Seismological Society of America* 86(6):1749–1759
- Andrus RD, Piratheepan P, Ellis BS, Zhang J, Juang CH (2004) Comparing liquefaction evaluation methods using penetration- V_S relationships. *Soil Dynamics and Earthquake Engineering* 24(9–10):713–721

- Bard PY, Duval AM, Bertrand E, Vassiliades JF, Vidal S, Foin P, Guéguen P, Thibault C, Guyet B, Dunand F, Bonnefoy-Claudet S, Méneroud JP, Vettori G (2005) Le risque sismique à Nice: Rapport méthodologique, résultats et perspectives opérationnelles. Final GEM-GEP report, LCPC, CGPC, METATTM, MEDD, CANCA, pp. 52
- Barker TG, Stevens JL (1983) Shallow shear wave velocity and Q structures at the El Centro strong motion accelerograph array. *Geophysical Research Letters* 10(9):853–856
- Beresnev IA, Wen KL (1996) Nonlinear soil response — a reality? *Bulletin of the Seismological Society of America* 86(6):1964–1978
- Berge-Thierry C, Cotton F, Scotti O, Griot-Pommera DA, Fukushima Y (2003) New empirical response spectral attenuation laws for moderate European earthquakes. *Journal of Earthquake Engineering* 7(2):193–222
- Bernreuter DL, Chen JC, Savy JB (1986) A methodology to correct for the effect of the local site's characteristics in seismic hazard analysis. In: *Proceedings of the Third U.S. National Conference on Earthquake Engineering*, vol I, pp 245–255
- Boore DM (2003) Simulation of ground motion using the stochastic method. *Pure and Applied Geophysics* 160(3–4):635–676, DOI 10.1007/PL00012553
- Boore DM (2004) Can site response be predicted? *Journal of Earthquake Engineering* 8(Special issue 1):1–42
- Boore DM (2005) SMSIM — Fortran programs for simulating ground motions from earthquakes: Version 2.3 — A revision of OFR 96-80-A. Open-File Report 00-509, United States Geological Survey, modified version, describing the program as of 15 August 2005 (Version 2.30).
- Boore DM, Atkinson GM (2007) Boore-Atkinson NGA ground motion relations for the geometric mean horizontal component of peak and spectral ground motion parameters. Report 2007/01, PEER
- Boore DM, Atkinson GM (2008) Ground-motion prediction equations for the average horizontal component of PGA, PGV, and 5%-damped PSA at spectral periods between 0.01 s and 10.0 s. *Earthquake Spectra* 24(1):99–138, DOI 10.1193/1.2830434
- Boore DM, Joyner WB (1991) Estimation of ground motion at deep-soil sites in eastern North America. *Bulletin of the Seismological Society of America* 81(6):2167–2185

- Boore DM, Joyner WB (1997) Site amplifications for generic rock sites. *Bulletin of the Seismological Society of America* 87(2):327–341
- Borcherdt RD (1994) Estimates of site-dependent response spectra for design (methodology and justification). *Earthquake Spectra* 10(4):617–653
- BRGM (2008a) Carte géologique imprimée. URL <http://infoterre.brgm.fr/>
- BRGM (2008b) La Banque du Sous-Sol. URL <http://infoterre.brgm.fr/>
- Campbell KW, Bozorgnia Y (2008) NGA ground motion model for the geometric mean horizontal component of PGA, PGV, PGD and 5% damped linear elastic response spectra for periods ranging from 0.01 to 10 s. *Earthquake Spectra* 24(1):139–171, DOI 10.1193/1.2857546
- Chandler AM, Lam NTK, Tsang HH (2005) Shear wave velocity modelling in crustal rock for seismic hazard analysis. *Soil Dynamics and Earthquake Engineering* 25(2):167–185
- Chandler AM, Lam NTK, Tsang HH (2006) Near-surface attenuation modelling based on rock shear-wave velocity profile. *Soil Dynamics and Earthquake Engineering* 26(11):1004–1014
- Chiou BSJ, Youngs RR (2008) An NGA model for the average horizontal component of peak ground motion and response spectra. *Earthquake Spectra* 24(1):173–215, DOI 10.1193/1.2894832
- Comité Européen de Normalisation (CEN) (2005) Eurocode 8, Design of structures for earthquake resistance — part 1: General rules, seismic actions and rules for buildings. European Standard NF EN 1998-1
- Cotton F, Scherbaum F, Bommer JJ, Bungum H (2006) Criteria for selecting and adjusting ground-motion models for specific target regions: Application to central Europe and rock sites. *Journal of Seismology* 10(2):137–156, DOI 10.1007/s10950-005-9006-7
- Douglas J (2003) Earthquake ground motion estimation using strong-motion records: A review of equations for the estimation of peak ground acceleration and response spectral ordinates. *Earth-Science Reviews* 61(1–2):43–104
- Dowrick DJ (2003) *Earthquake Risk Reduction*. John Wiley & Sons Ltd, Chichester, United Kingdom
- Draper NR, Smith H (1998) *Applied Regression Analysis*, 3rd edn. John Wiley & Sons
- Drouet S, Chevrot S, Cotton F, Souriau A (2008) Simultaneous inversion of source spectra, attenuation parameters, and site responses: Application to the data of the French

- Accelerometric Network. *Bulletin of the Seismological Society of America* 98(1):198–219, DOI 10.1785/0120060215
- Duval AM, Bard PY, Le Brun B, Lacave-Lachet C, Riepl J, Hatzfeld D (2001) H/V technique for site response analysis synthesis of data from various surveys. *Bollettino di Geofisica Teorica ed Applicata* 42(3–4):267–280
- European-Mediterranean Seismological Centre (2007) Euro-Med accelerometric networks in the Euro-Med region. URL <http://www.emsc-csem.org/index.php?page=projects&sub=accelero>
- Field EH (2000) A modified ground-motion attenuation relationship for southern California that accounts for detailed site classification and a basin-depth effect. *Bulletin of the Seismological Society of America* 90(6B):S209–S221
- Fukushima Y, Bonilla LF, Scotti O, Douglas J (2007) Site classification using horizontal-to-vertical response spectral ratios and its impact when deriving empirical ground motion prediction equations. *Journal of Earthquake Engineering* 11(5):712–724, DOI 10.1080/13632460701457116
- Fuller WA (1987) *Measurement Error Models*. John Wiley & Sons, New York, USA
- Fumal TE, Tinsley JC (1985) Mapping shear-wave velocities of near-surface geologic materials. In: *Evaluating Earthquake Hazards in the Los Angeles Region — An Earth Science Perspective*, no. 1360 in U.S. Geological Survey Professional Paper, United States Government Printing Office, Washington, pp 127–149
- Groupe de Travail RAP (2007) *Reconnaissance géotechnique des stations du RAP: Phase pilote*. Tech. rep., Réseau Accélérométrique Permanent, UMR LGIT, BRGM, CETE Nice, IRSN, IRD, LCPC
- Hasancebi N, Ulusay R (2007) Empirical correlations between shear wave velocity and penetration resistance for ground shaking assessments. *Bulletin of Engineering Geology and the Environment* 66(2):203–213, DOI 10.1007/s10064-006-0063-0
- Huo J, Hu Y (1991) Attenuation laws considering the randomness of magnitude and distance. *Earthquake Research in China* 5(1):17–36
- Idriss IM (2008) An NGA empirical model for estimating the horizontal spectral values generated by shallow crustal earthquakes. *Earthquake Spectra* 24(1):217–242, DOI 10.1193/1.2924362

- Joyner WB, Fumal TE (1984) Use of measured shear-wave velocity for predicting geologic site effects on strong ground motion. In: Proceedings of Eighth World Conference on Earthquake Engineering, vol II, pp 777–783
- Joyner WB, Warrick RE, Fumal TE (1981) The effect of quaternary alluvium on strong ground motion in the Coyote Lake, California, earthquake of 1979. Bulletin of the Seismological Society of America 71(4):1333–1349
- Kamiyama M, Yanagisawa E (1986) A statistical model for estimating response spectra of strong earthquake ground motions with emphasis on local soil conditions. Soils and Foundations 26(2):16–32
- Laske G, Dziewonski A, Masters G (2005) The Reference Earth Model website. On Internet at: <http://mahi.ucsd.edu/Gabi/rem.html>
- Ohta Y, Goto N (1978) Empirical shear wave velocity equations in terms of characteristic soil indexes. Earthquake Engineering and Structural Dynamics 6:167–187
- Parolai S, Bormann P, Milkereit C (2002) New relationship between V_s , thickness of sediments, and resonance frequency calculated by the H/V ratio of seismic noise for the Cologne area (Germany). Bulletin of the Seismological Society of America 92(6):2521–2527
- Rhoades DA (1997) Estimation of attenuation relations for strong-motion data allowing for individual earthquake magnitude uncertainties. Bulletin of the Seismological Society of America 87(6):1674–1678
- Rodriguez-Marek A, Bray JD, Abrahamson N (1999) Task 3: Characterization of site response general site categories. PEER Report 1999/03, Pacific Earthquake Engineering Research Center, College of Engineering, University of California, Berkeley
- ROSRINE (2008) ResOlution of Site Response Issues from the Northridge Earthquake. URL <http://gees.usc.edu/ROSRINE/>
- Silva W, Darragh R, Gregor N, Martin G, Abrahamson N, Kircher C (1998) Reassessment of site coefficients and near-fault factors for building code provisions. Tech. Rep. Program Element II: 98-HQ-GR-1010, Pacific Engineering and Analysis, El Cerrito, USA
- Souriau A, Granet M (1995) A tomographic study of the lithosphere beneath the Pyrenees from local and teleseismic data. Journal of Geophysical Research 100(B9):18,117–18,134

- Souriau A, Roullé A, Ponsolles C (2007) Site effects in the city of Lourdes, France, from H/V measurements: Implications for seismic-risk evaluation. *Bulletin of the Seismological Society of America* 97(6):2118–2136, DOI 10.1785/0120060224
- Spudich P, Joyner WB, Lindh AG, Boore DM, Margaris BM, Fletcher JB (1999) SEA99: A revised ground motion prediction relation for use in extensional tectonic regimes. *Bulletin of the Seismological Society of America* 89(5):1156–1170
- Vallon M (1999) Estimation de l'épaisseur d'alluvions quaternaires dans la cuvette grenobloise par inversion des anomalies gravimétriques. Tech. rep., Université Joseph Fourier & Laboratoire de Glaciologie et Géophysique de l'Environnement du C.N.R.S., Grenoble, France, in French
- Wald DJ, Allen TI (2007) Topographic slope as a proxy for seismic site conditions and amplification. *Bulletin of the Seismological Society of America* 97(5):1379–1395, DOI 10.1785/0120060267
- Wei BZ, Pezeshk S, Chang TS, Hall KH, Liu HP (1996) An empirical method to estimate shear wave velocity of soils in the New Madrid seismic zone. *Soil Dynamics and Earthquake Engineering* 15(6):399–408
- Wills CJ, Petersen M, Bryant WA, Reichle M, Saucedo GJ, Tan S, Taylor G, Treiman J (2000) A site-conditions map for California based on geology and shear-wave velocity. *Bulletin of the Seismological Society of America* 90(6B):S187–S208

List of Figures

1	Histograms showing the characteristics of the 858 shear-wave velocity profiles used to derive statistics for the generation of stochastic profiles.	26
2	Maximum shear-wave velocity within the profile against depth of profile for the 858 shear-wave velocity profiles. This graph only goes up to 300 m due to a limited number of deeper profiles.	27
3	Normalized slopes against depth for the 858 shear-wave velocity profiles. This graph only goes up to 200 m due to few slopes from greater depths.	28
4	Summary of method used to generate the velocity profiles, using various types of information depending on the depth.	29
5	Estimated mean shear-wave velocity profiles for the 14 selected RAP stations (solid lines) and their 10 and 90% confidence limits (dashed lines) using the method developed within this article.	30
6	Mean site amplification curves (solid lines) and their 10 and 90% confidence limits estimated for the 14 RAP stations using the shear-wave velocity profiles derived in this study and presented in Figure 5.	31
7	Comparison between the computed mean site amplifications (solid lines) and their 10 and 90% confidence limits (dashed lines) for the NALS station when the uncertainty in κ estimated from the $V_{s,30}$ is neglected (left-hand figure) and when it is considered (right-hand figure).	32
8	Comparison between the computed mean site amplifications (solid lines) and their 10 and 90% confidence limits (dashed lines) for the OGSR station when the uncertainty in κ estimated from the $V_{s,30}$ is neglected (left-hand figure) and when it is considered (right-hand figure).	33
9	Comparison between the site amplification curves computed in this study and their 10 and 90% confidence limits (solid lines) and the site amplifications (and their $\pm 1.28\sigma$ confidence limits corresponding to the 10 and 90% confidence limits for a normal distribution) computed by source-path-site inversion by Drouet et al (2008) (dashed lines) for the seven common stations.	34
10	Mean site amplification curves for the NALS station (solid lines) and their 10 and 90% confidence limits (dashed lines) for four sets of constraints: I) near-surface shear-wave velocity profile, depth to bedrock and crustal structure; II) V_0 , $V_{s,30}$, depth to bedrock and crustal structure; III) V_0 , $V_{s,30}$ and crustal structure; and IV) $V_{s,30}$ and crustal structure.	35

11	Mean site amplification curves for the OGSR station (solid lines) and their 10 and 90% confidence limits (dashed lines) for four sets of constraints: I) near-surface shear-wave velocity profile, depth to bedrock and crustal structure; II) V_0 , $V_{s,30}$, depth to bedrock and crustal structure; III) V_0 , $V_{s,30}$ and crustal structure; and IV) $V_{s,30}$ and crustal structure.	36
12	Generated velocity profiles for the four soil classes and their 10 and 90% confidence limits (dashed lines). The grey solid line represents the velocity profile developed using the generic model of Cotton et al (2006) based on $V_{s,30}$	37
13	Amplification curves for the four soil classes, and their 10 and 90% confidence limits (dashed lines). The grey solid line represents the amplification curve that was computed using the velocity profile developed using the generic model of Cotton et al (2006) based on $V_{s,30}$	38
14	Comparison between the mean amplification curve and its 10 and 90% confidence limits computed using the one-quarter wavelength method (thick lines) and the mean amplification curve and its 10 and 90% confidence limits computed using the Haskell-Thompson method (thin lines) for the OGDH station. The profiles simulated using the Monte Carlo technique developed in this article are used for both computations.	39

Figure 1: Histograms showing the characteristics of the 858 shear-wave velocity profiles used to derive statistics for the generation of stochastic profiles.

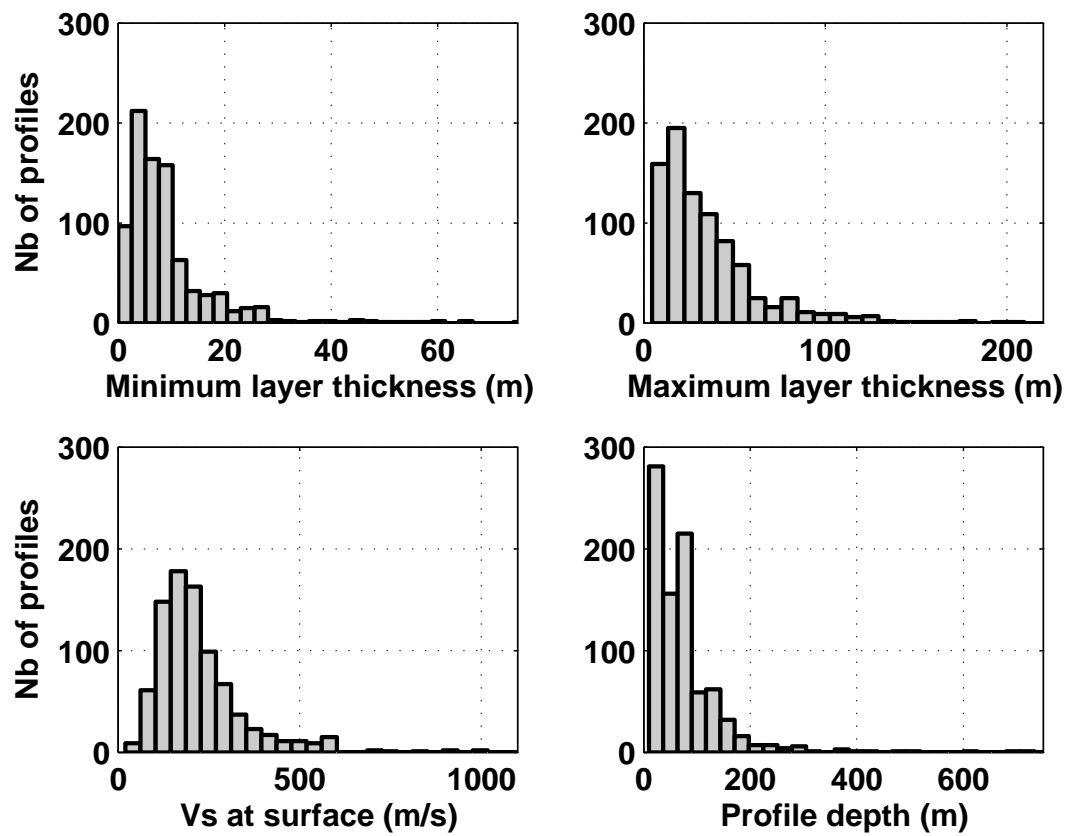


Figure 2: Maximum shear-wave velocity within the profile against depth of profile for the 858 shear-wave velocity profiles. This graph only goes up to 300m due to a limited number of deeper profiles.

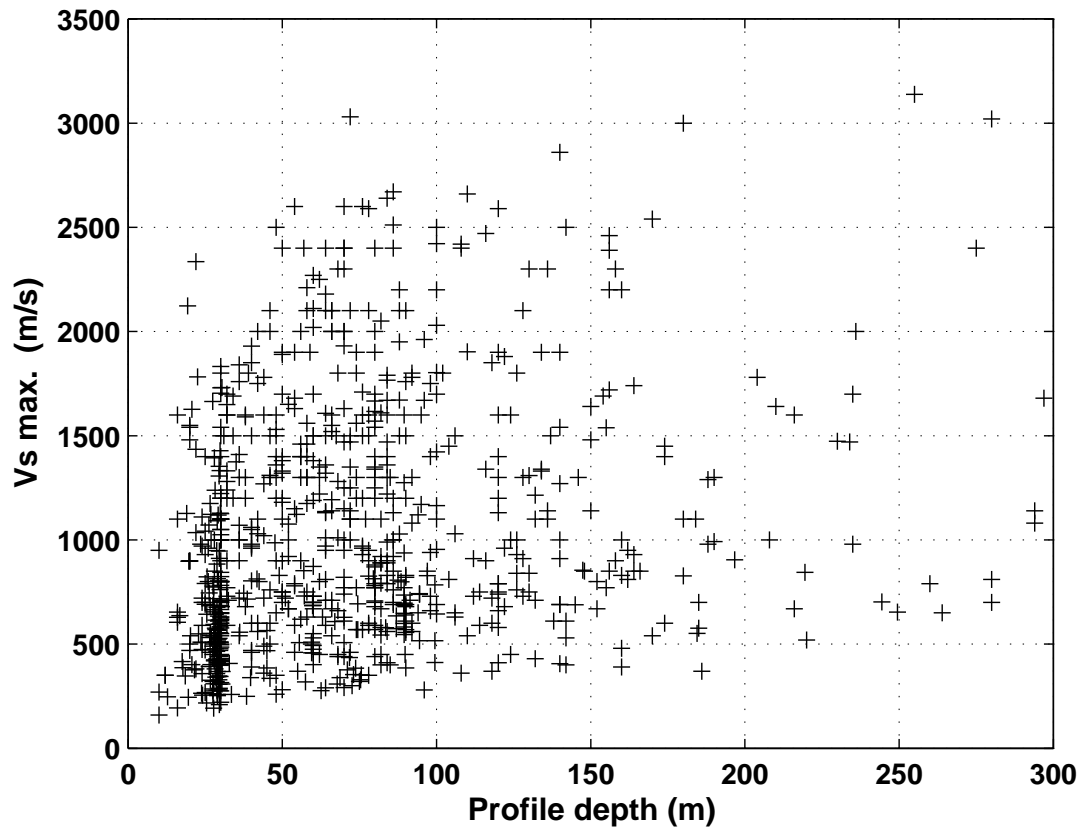


Figure 3: Normalized slopes against depth for the 858 shear-wave velocity profiles. This graph only goes up to 200m due to few slopes from greater depths.

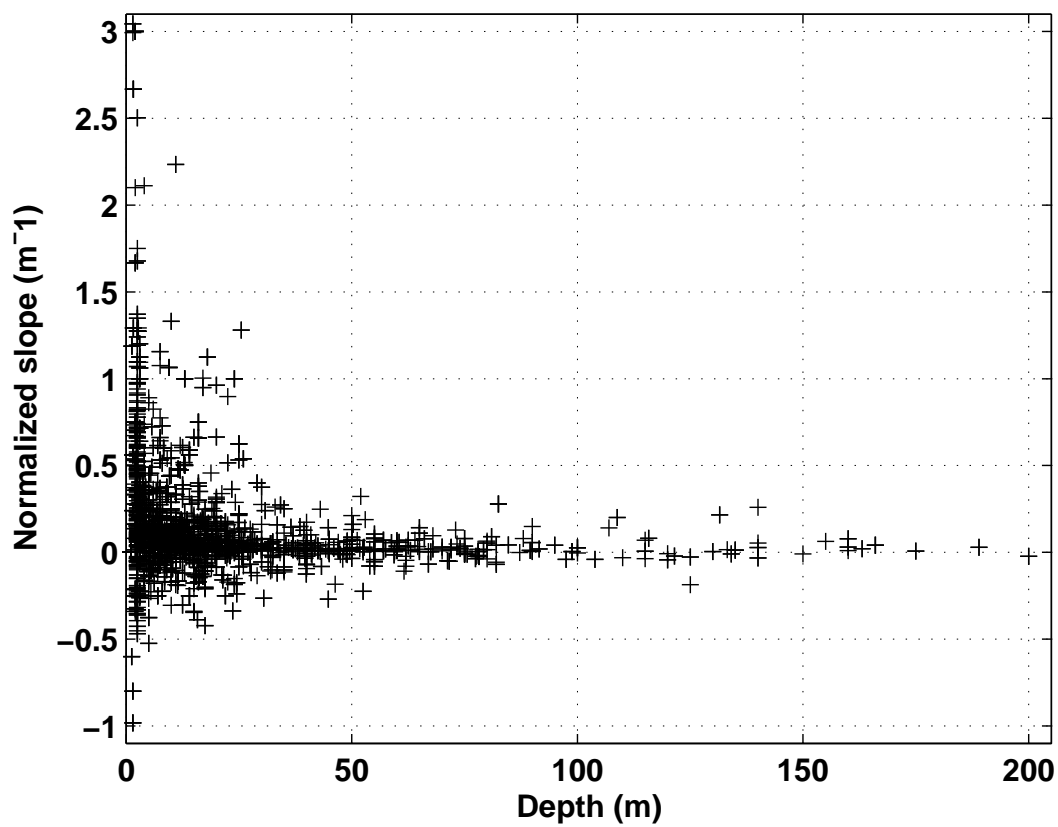


Figure 4: Summary of method used to generate the velocity profiles, using various types of information depending on the depth.

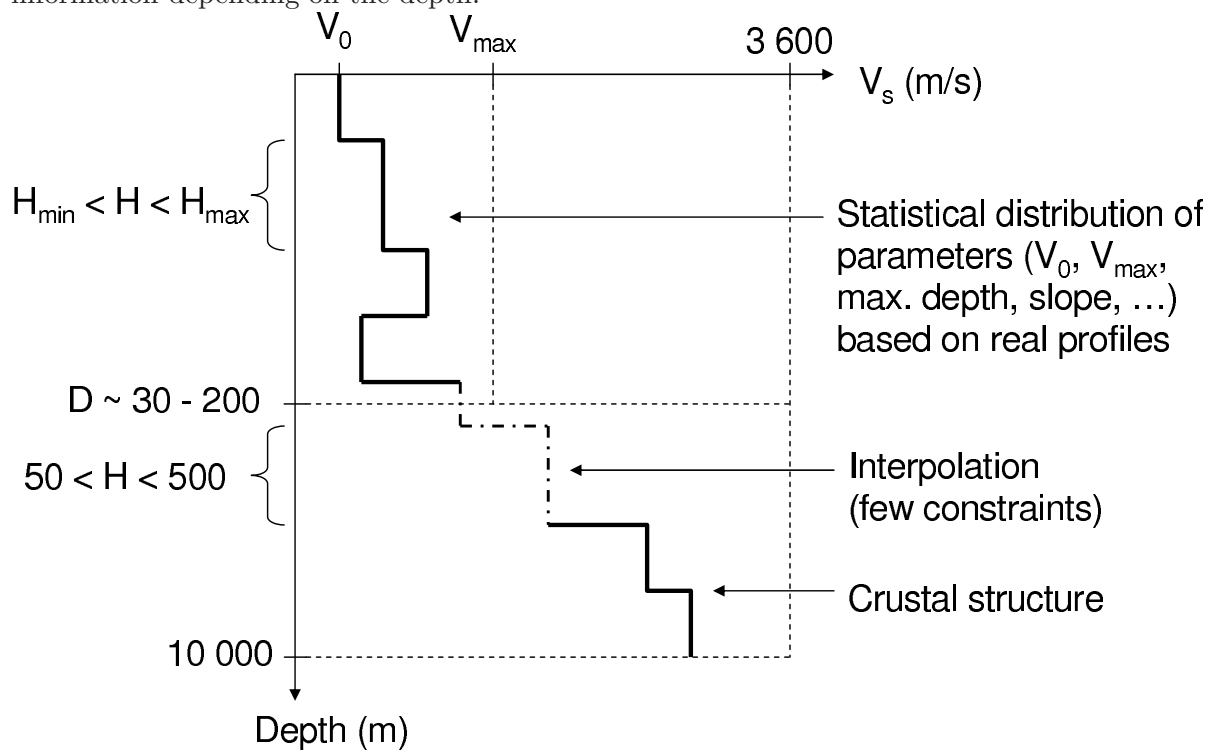


Figure 5: Estimated mean shear-wave velocity profiles for the 14 selected RAP stations (solid lines) and their 10 and 90% confidence limits (dashed lines) using the method developed within this article.

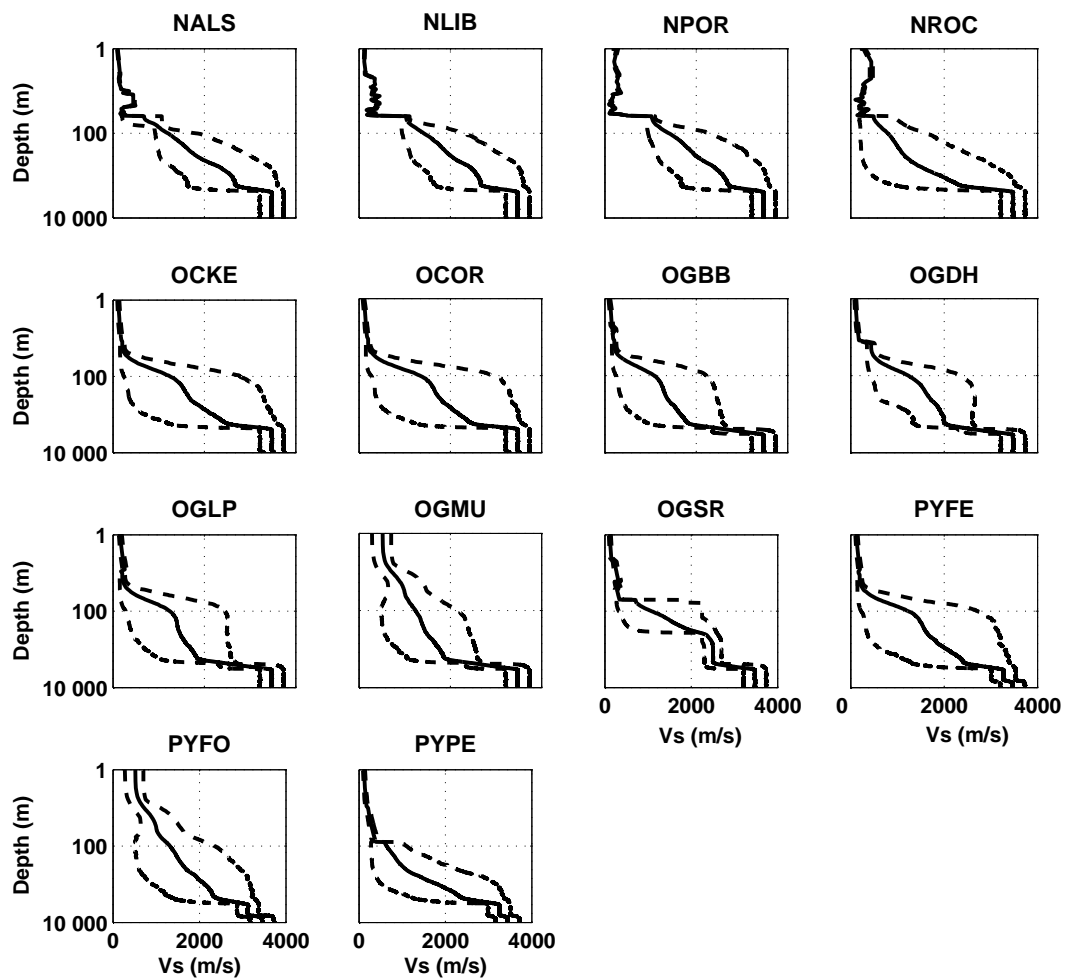


Figure 6: Mean site amplification curves (solid lines) and their 10 and 90% confidence limits estimated for the 14 RAP stations using the shear-wave velocity profiles derived in this study and presented in Figure 5.

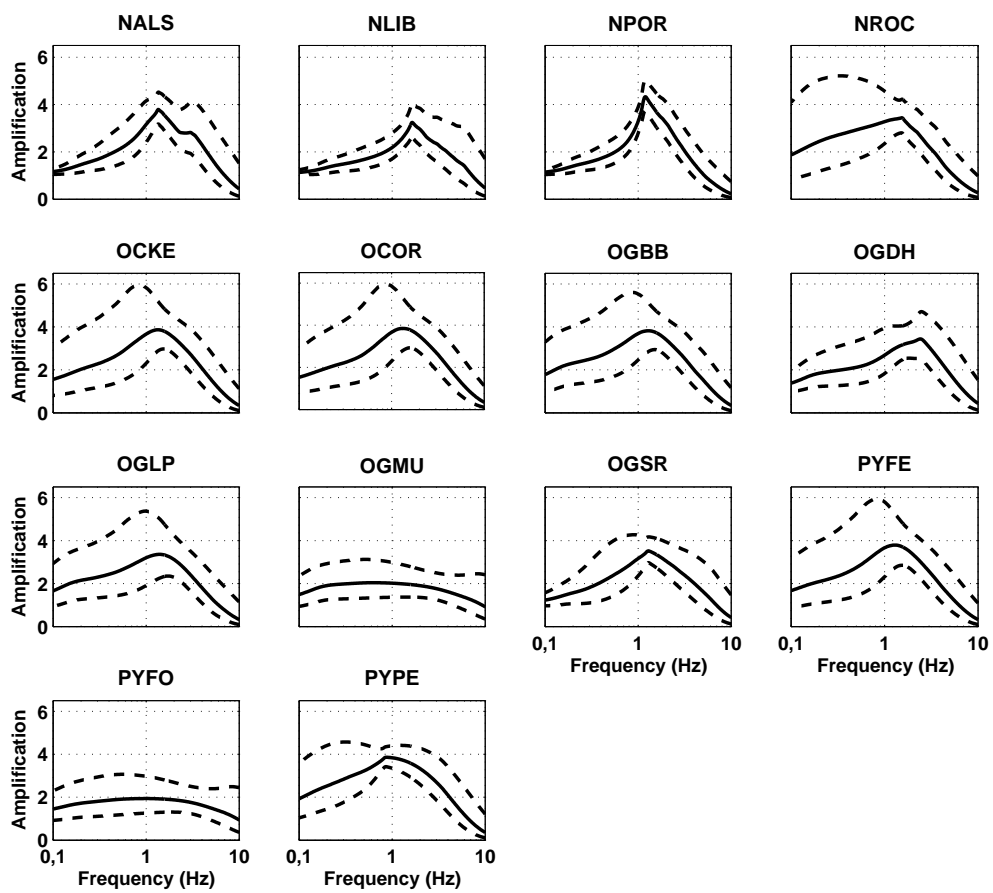


Figure 7: Comparison between the computed mean site amplifications (solid lines) and their 10 and 90% confidence limits (dashed lines) for the NALS station when the uncertainty in κ estimated from the $V_{s,30}$ is neglected (left-hand figure) and when it is considered (right-hand figure).

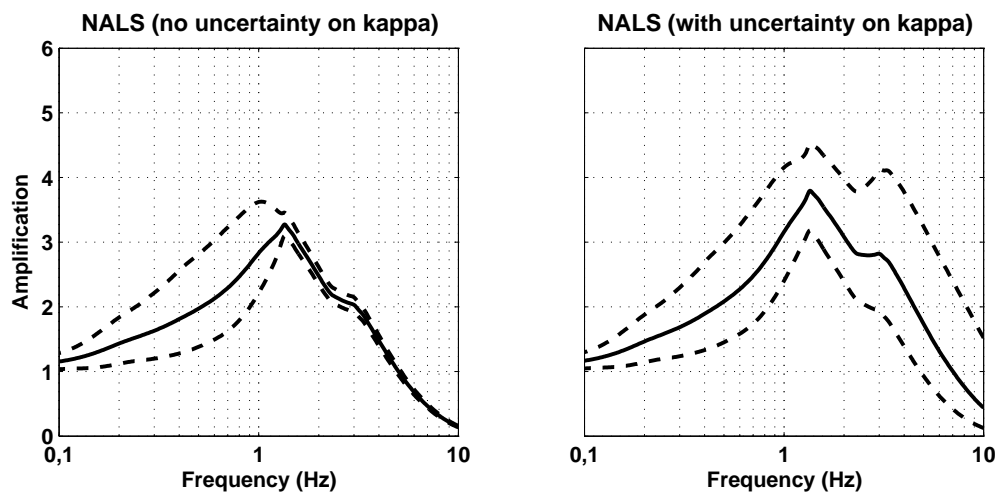


Figure 8: Comparison between the computed mean site amplifications (solid lines) and their 10 and 90% confidence limits (dashed lines) for the OGSR station when the uncertainty in κ estimated from the $V_{s,30}$ is neglected (left-hand figure) and when it is considered (right-hand figure).

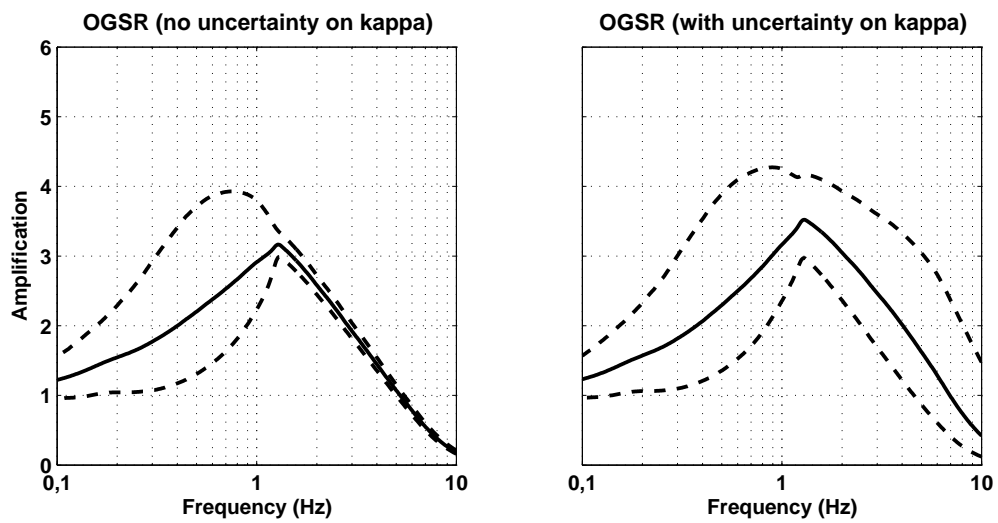


Figure 9: Comparison between the site amplification curves computed in this study and their 10 and 90% confidence limits (solid lines) and the site amplifications (and their $\pm 1.28\sigma$ confidence limits corresponding to the 10 and 90% confidence limits for a normal distribution) computed by source-path-site inversion by Drouet et al (2008) (dashed lines) for the seven common stations.

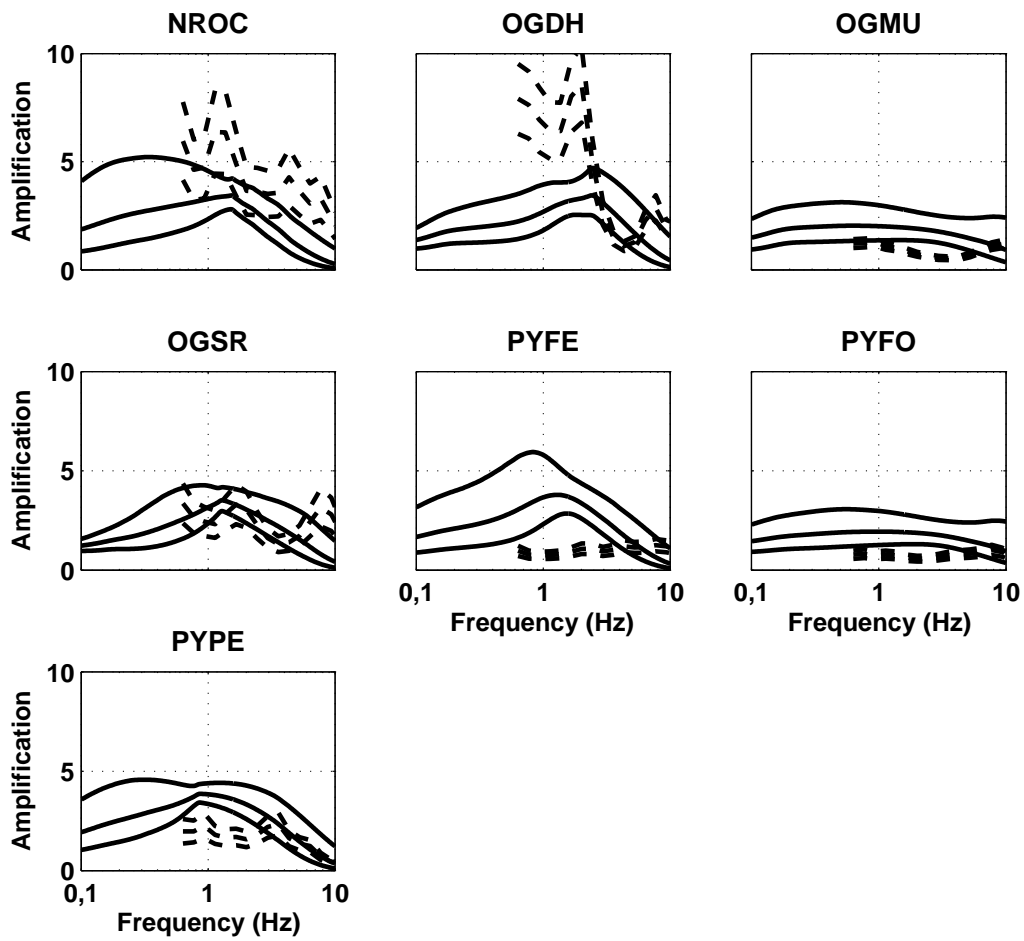


Figure 10: Mean site amplification curves for the NALS station (solid lines) and their 10 and 90% confidence limits (dashed lines) for four sets of constraints: I) near-surface shear-wave velocity profile, depth to bedrock and crustal structure; II) V_0 , $V_{s,30}$, depth to bedrock and crustal structure; III) V_0 , $V_{s,30}$ and crustal structure; and IV) $V_{s,30}$ and crustal structure.

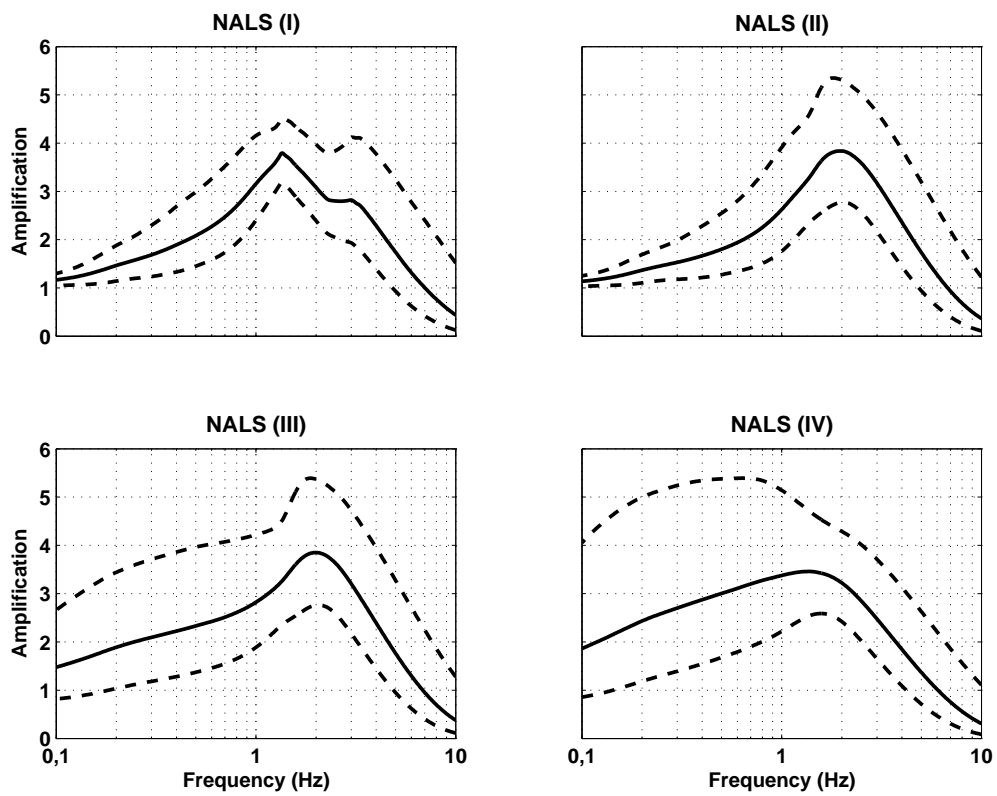


Figure 11: Mean site amplification curves for the OGSR station (solid lines) and their 10 and 90% confidence limits (dashed lines) for four sets of constraints: I) near-surface shear-wave velocity profile, depth to bedrock and crustal structure; II) V_0 , $V_{s,30}$, depth to bedrock and crustal structure; III) V_0 , $V_{s,30}$ and crustal structure; and IV) $V_{s,30}$ and crustal structure.

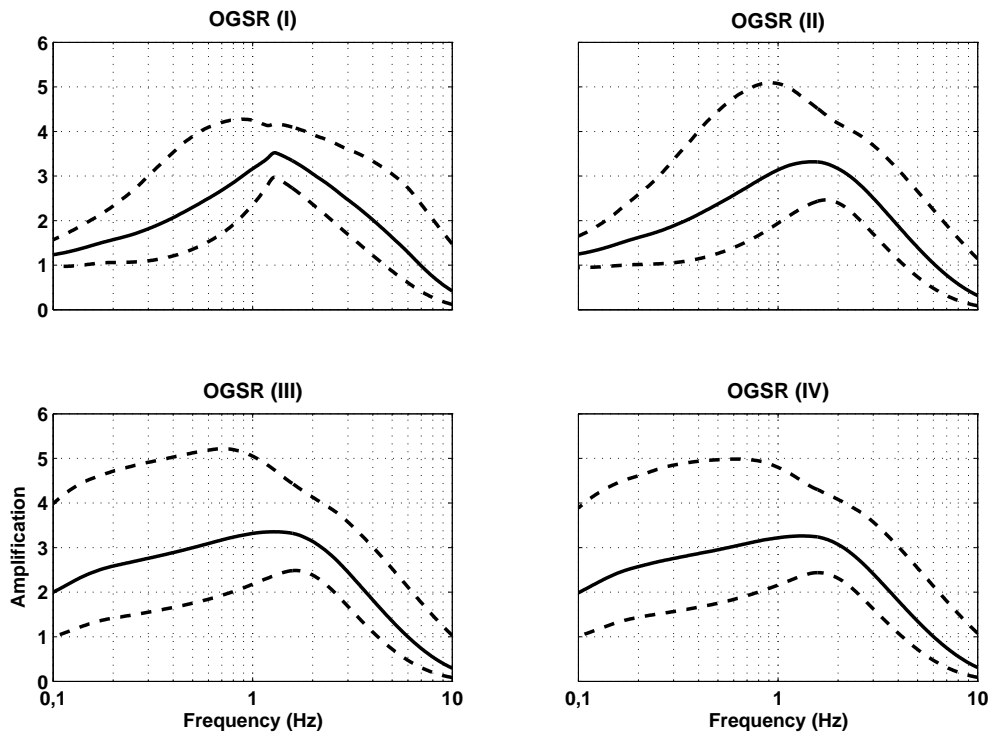


Figure 12: Generated velocity profiles for the four soil classes and their 10 and 90% confidence limits (dashed lines). The grey solid line represents the velocity profile developed using the generic model of Cotton et al (2006) based on $V_{s,30}$.

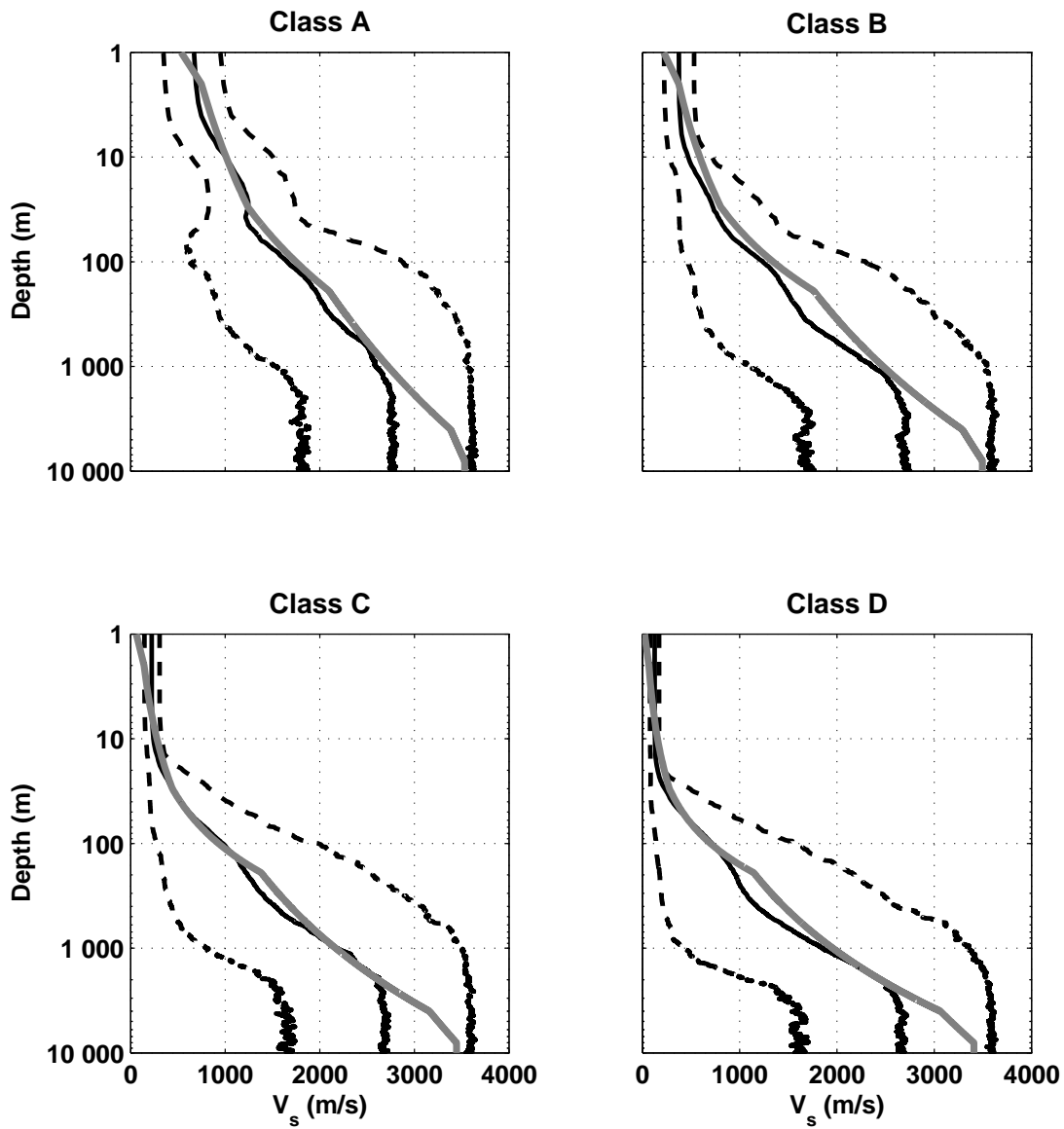


Figure 13: Amplification curves for the four soil classes, and their 10 and 90% confidence limits (dashed lines). The grey solid line represents the amplification curve that was computed using the velocity profile developed using the generic model of Cotton et al (2006) based on $V_{s,30}$.

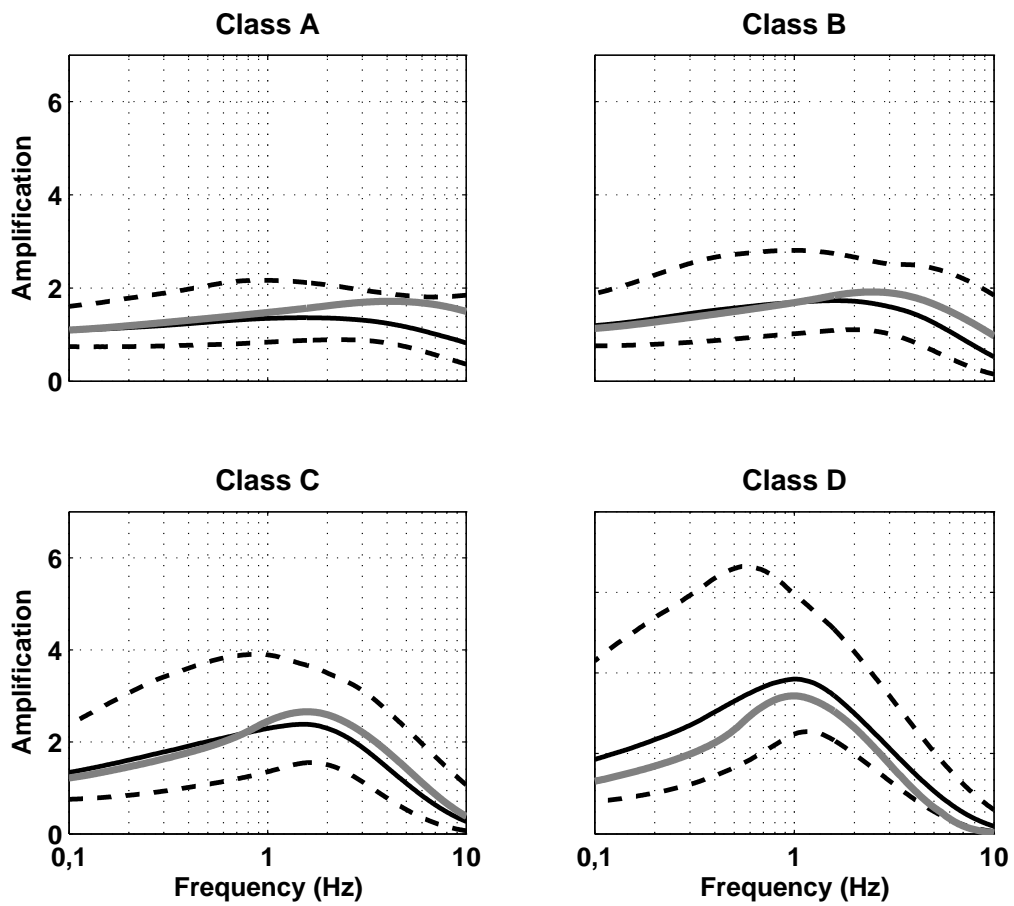
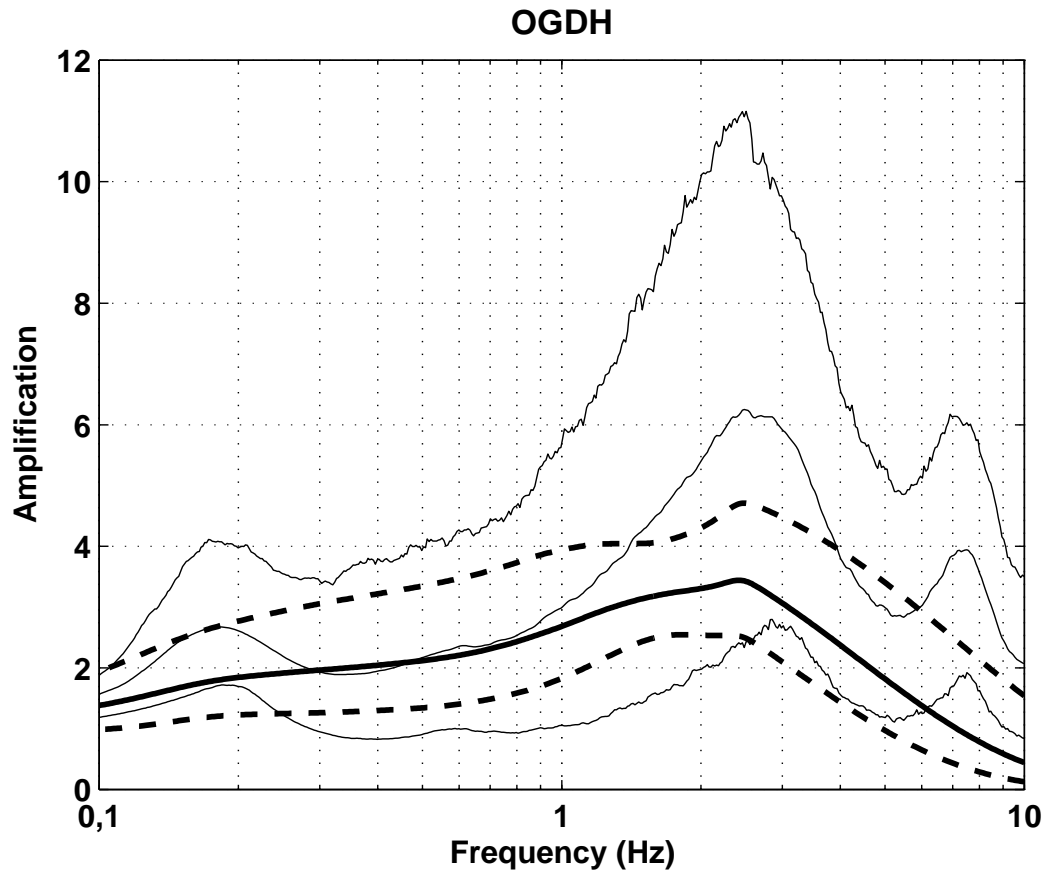


Figure 14: Comparison between the mean amplification curve and its 10 and 90% confidence limits computed using the one-quarter wavelength method (thick lines) and the mean amplification curve and its 10 and 90% confidence limits computed using the Haskell-Thompson method (thin lines) for the OGDH station. The profiles simulated using the Monte Carlo technique developed in this article are used for both computations.



List of Tables

1	Information available to constrain shear-wave velocity and density profiles down to a few kms.	41
2	Correlation coefficients between different characteristics of the observed profiles.	42
3	Strong-motion stations of the RAP considered in this study and the information available to constrain the shear-wave velocity and density profiles down to a few kms. Italics indicate those data that were not used to constrain the profiles in this study.	43
4	Computed mean $V_{s,\frac{1}{4}}$ and its 10 and 90th percentile confidence limits for the 14 RAP stations and the four EC8 site classes for different spectral periods. . . .	44

Table 1: Information available to constrain shear-wave velocity and density profiles down to a few kms.

Type of information	Examples
Soil profile	BRGM (2008b)
Crustal structure	Souriau and Granet (1995), CRUST2.0 (Laske et al, 2005)
Generic V_s profile	Boore and Joyner (1991), Anderson et al (1996), Boore and Joyner (1997), Parolai et al (2002), Chandler et al (2005), Chandler et al (2006), Cotton et al (2006)
Measured V_s profile	ROSRINE (2008)
Near-surface geology	National/region/local geological maps (BRGM, 2008a), Wills et al (2000)
Microtremor measurements	Souriau et al (2007)
Site class	Borcherdt (1994), Comité Européen de Normalisation (CEN) (2005)
Standard penetration test (SPT)	Wei et al (1996), Hasancebi and Ulusay (2007)
Cone penetration test (CPT)	Andrus et al (2004)
Topographic slope	Wald and Allen (2007)
Depth to bedrock (from, e.g., Bouguer gravity data or H/V results)	Vallon (1999), Parolai et al (2002)

Table 2: Correlation coefficients between different characteristics of the observed profiles.

	V_s	Depth to top of layer	Layer thickness	Slope
V_s	1	0.4519	0.4152	-0.2089
Depth to top of layer		1	0.7295	-0.2505
Layer thickness			1	-0.1861
Slope				1

Table 3: Strong-motion stations of the RAP considered in this study and the information available to constrain the shear-wave velocity and density profiles down to a few kms. Italics indicate those data that were not used to constrain the profiles in this study.

Station	Latitude	Longitude	Information available
NALS	43.699N	7.258E	Surface geology, soil profile down to 39 m, SPT down to 39 m, <i>H/V noise spectrum (Bard et al, 2005)</i> , crustal structure (Laske et al, 2005), topographic slope (Wald and Allen, 2007), <i>site class (soil)</i>
NLIB	43.710N	7.264E	Surface geology, soil profile down to 39 m, SPT down to 39 m, <i>H/V noise spectrum (Bard et al, 2005)</i> , crustal structure (Laske et al, 2005), topographic slope (Wald and Allen, 2007), <i>site class (soil)</i>
NPOR	43.700N	7.286E	Surface geology, soil profile down to 39 m, SPT down to 39 m, <i>H/V noise spectrum (Bard et al, 2005)</i> , crustal structure (Laske et al, 2005), topographic slope (Wald and Allen, 2007), <i>site class (soil)</i>
NROC	43.716N	7.293E	Surface geology, soil profile down to 39 m, SPT down to 39 m, <i>H/V noise spectrum (Bard et al, 2005)</i> , crustal structure (Laske et al, 2005), topographic slope (Wald and Allen, 2007), <i>site class (soil)</i>
OCKE	45.771N	3.088E	Surface geology, soil profile down to 12 m, SPT down to 9 m, <i>H/V noise spectrum</i> , crustal structure (Laske et al, 2005), topographic slope (Wald and Allen, 2007), <i>site class (soil)</i>
OCOR	45.798N	3.028E	Surface geology, soil profile down to 11 m, <i>H/V noise and earthquake spectra</i> , crustal structure (Laske et al, 2005), topographic slope (Wald and Allen, 2007), <i>site class (rock)</i>
OGBB	44.281N	5.26E	Surface geology, soil profile down to 12.2 m, crustal structure (Laske et al, 2005), topographic slope (Wald and Allen, 2007), <i>site class (rock)</i>
OGDH	45.182N	5.737E	Surface geology, soil profile down to 15 m, SPT down to 39 m, <i>H/V noise and earthquake spectra</i> , depth to bedrock (Vallon, 1999), crustal structure (Laske et al, 2005), topographic slope (Wald and Allen, 2007), <i>site class (soil)</i>
OGLP	44.307N	4.69E	Surface geology, soil profile down to 10 m, SPT down to 13 m, <i>H/V noise spectrum</i> , crustal structure (Laske et al, 2005), topographic slope (Wald and Allen, 2007), <i>site class (soil)</i>
OGMU	45.195N	5.727E	Surface geology, <i>H/V noise and earthquake spectra</i> , crustal structure (Laske et al, 2005), topographic slope (Wald and Allen, 2007), <i>site class (rock)</i>
OGSR	45.193N	5.74E	Surface geology, soil profile down to 50 m, <i>H/V noise and earthquake spectra</i> , depth to bedrock (Vallon, 1999), crustal structure (Laske et al, 2005), topographic slope (Wald and Allen, 2007), <i>site class (soil)</i>
PYFE	42.814N	2.507E	Surface geology, soil profile down to 11 m, <i>H/V noise and earthquake spectra</i> , crustal structure (Laske et al, 2005), topographic slope (Wald and Allen, 2007), <i>site class (soil)</i>
PYFO	42.968N	1.607E	Surface geology, <i>H/V noise and earthquake spectra</i> , crustal structure (Laske et al, 2005), topographic slope (Wald and Allen, 2007), <i>site class (soil)</i>
PYPE	42.673N	2.878E	Surface geology, soil profile down to 78.5 m, <i>H/V noise and earthquake spectra</i> , crustal structure (Laske et al, 2005), topographic slope (Wald and Allen, 2007), <i>site class (soil)</i>

Table 4: Computed mean $V_{s, \frac{1}{4}}$ and its 10 and 90th percentile confidence limits for the 14 RAP stations and the four EC8 site classes for different spectral periods.

Station	Statistical measure	$V_{s, \frac{1}{4}}$						
		0.1 s	0.2 s	0.5 s	1 s	2 s	5 s	10 s
NALS	mean	175	211	959	1731	2528	2920	3203
	10th percentile	141	193	446	782	1215	2234	2730
	90th percentile	209	275	1768	2696	3216	3353	3550
NLIB	mean	241	384	1306	1958	2676	2981	3235
	10th percentile	208	291	735	1037	1513	2358	2793
	90th percentile	272	571	2191	2923	3328	3398	3572
NPOR	mean	209	177	981	1761	2549	2929	3207
	10th percentile	196	167	567	924	1416	2320	2774
	90th percentile	220	187	1724	2666	3200	3347	3547
NROC	mean	252	269	637	1051	1928	2680	3083
	10th percentile	235	220	208	210	221	358	1603
	90th percentile	266	406	1692	2613	3173	3335	3539
OCKE	mean	151	207	889	1477	2321	2849	3186
	10th percentile	114	133	153	210	283	1034	2065
	90th percentile	195	714	2298	2965	3350	3411	3582
OCOR	mean	149	209	950	1534	2356	2862	3190
	10th percentile	109	129	150	221	305	1097	2095
	90th percentile	193	780	2353	2988	3362	3413	3581
OGBB	mean	157	208	743	1133	1635	2559	3024
	10th percentile	116	134	154	208	275	686	1862
	90th percentile	197	620	1724	2146	2831	3201	3475
OGDH	mean	129	317	1023	1472	2034	2724	3107
	10th percentile	96	181	318	433	762	1918	2483
	90th percentile	194	808	1904	2259	2910	3231	3489
OGLP	mean	202	328	950	1295	1809	2632	3058
	10th percentile	153	151	165	238	337	1025	2036
	90th percentile	281	1166	1974	2281	2926	3236	3491
OGMU	mean	939	1122	1345	1549	2061	2734	3110
	10th percentile	514	517	503	529	636	1647	2348
	90th percentile	1722	2046	2323	2466	3056	3288	3517
OGSR	mean	206	256	1018	1755	2369	2857	3172
	10th percentile	149	192	250	377	1327	2221	2726
	90th percentile	267	522	1755	2227	2889	3221	3482
PYFE	mean	163	214	882	1415	2042	2680	3078
	10th percentile	125	133	146	194	268	661	1813
	90th percentile	207	791	2232	2805	3166	3319	3529
PYFO	mean	953	1185	1520	1842	2289	2749	3104
	10th percentile	512	521	524	560	710	1586	2294
	90th percentile	1844	2329	2810	3030	3198	3322	3529
PYPE	mean	160	217	429	779	1451	2399	2923
	10th percentile	115	157	227	257	290	536	1679
	90th percentile	206	283	950	2026	2748	3131	3429
EC8 class A	mean	1307	1633	2102	2408	2584	2526	2672
	10th percentile	662	645	787	991	1352	1628	1659
	90th percentile	2456	2946	3325	3464	3539	3421	3537
EC8 class B	mean	625	932	1422	1923	2306	2366	2558
	10th percentile	300	339	426	516	754	1279	1409
	90th percentile	1413	2144	2921	3256	3422	3367	3507
EC8 class C	mean	262	422	926	1477	2044	2254	2493
	10th percentile	154	173	203	263	351	891	1193
	90th percentile	537	1308	2485	3025	3309	3320	3482
EC8 class D	mean	127	139	389	811	1518	2023	2372
	10th percentile	79	79	82	95	128	205	708
	90th percentile	172	306	1550	2500	3042	3209	3423